CrystEngComm

PAPER

View Article Online
View Journal

Cite this: DOI: 10.1039/c5ce01973g

Ionothermal synthesis of FeAPO-5 in the presence of phosphorous acid

Eng-Poh Ng,*[a] Jia-Pei Ghoy,[a] Hussein Awala,[b] Aurélie Vicente,[b] Rohana Adnan,[a] Tau Chuan Ling[c] and Svetlana Mintova[b]

Received 9th October 2015,
Accepted 24th November 2015

DOI: 10.1039/c5ce01973g

www.rsc.org/crystengcomm

The ionothermal crystallization of FeAPO-5 molecular sieves in the presence of phosphorous acid (H_3PO_3) has been investigated. The use of H_3PO_3 enabled the formation of a metastable intermediate phase (FeNKX-2) that transforms into a more open-framework crystalline phase (FeAPO-5). The initial raw materials dissolved rapidly in the presence of the [bdmim]Cl polar ionic liquid, and the addition of the Fe^{3+} salt resulted in the crystallization of the FeNKX-2 intermediate. At this stage, the $[bdmim]^+$ cation did not play the role of a pore filler for the FeNKX-2 crystalline structure. Consecutive phase transformation from the FeNKX-2 to the FeAPO-5 phase occurred under prolonged ionothermal treatment, and during this stage, the tetrahedral Fe^{3+} species was found to not only participate in the construction of the FeAPO-5 framework but also act as an intermediary electron-transfer medium. The fast crystallization of FeAPO-5 was explained by the presence of Fe^{3+} as an intermediate electron-transfer medium promoting the fast release of phosphorus nutrients (P^{5+}) from the phosphite (P^{3+}) reservoir that were further required for the crystallization of the FeAPO-5 molecular sieves. The use of ionic liquids as dual solvents and templates in combination with H_3PO_3 as an alternative phosphorus source thus opens the possibility to synthesize other microporous materials *via* a phase transformation approach.

1. Introduction

The discovery of microporous aluminophosphates (AlPO-*n*) is considered as a breakthrough in zeolite science since they have wide applications as adsorbents,[1,2] catalysts,[3] membranes,[4] sensors,[5] *etc.*[6,7] Typically, these zeotype materials are prepared under hydrothermal conditions where phosphoric acid (H_3PO_4) is used as a source of phosphorus.

A new route for the hydrothermal synthesis of aluminophosphate materials based on phosphorous acid (H_3PO_3) as a source has also been reported.[8,9] H_3PO_3 is a moderately strong dibasic acid (pK_{a1} = 1.80, pK_{a2} = 6.15) with the structural formula $HPO(OH)_2$.[10] The $HPO(OH)_2$ species usually exists in equilibrium with a minor tautomer $P(OH)_3$ where the phosphorus ion exists in the P^{3+} state. H_3PO_3 was found to behave differently from H_3PO_4 during the crystallization of aluminophosphite and/or aluminophosphate molecular sieves.[11] In the synthesis process using H_3PO_3 as the phosphorus source, NKX-2 is formed as an aluminophosphite intermediate (180 °C, 6 days), whereas this intermediate phase is not observed in the H_3PO_4-containing route.[8] The transformation of microporous aluminophosphates including SAPO-46, AlPO-47, AlPO-41, SAPO-31, AlPO-11, AlPO-5 and AlPO-CJ2 from NKX-2 has been observed but it requires long crystallization time (7–16 days) and high temperature (*ca.* 200 °C) due to the slow release of phosphorus nutrients (P^{5+}) that are required for the crystallization and growth of aluminophosphates.[8,9,12]

Recently, ionothermal synthesis using ionic liquids as solvents and templates has been developed to prepare aluminophosphate molecular sieves.[13–16] The synthesis can be performed in either open or closed vessels. Furthermore, by using the ionothermal synthesis method and phosphorous acid (H_3PO_3), NKX-2 can be obtained within 3 h, which is faster than the time needed for the hydrothermal approach (6 days).[17]

Isomorphous substitution of transition metals into the framework sites of aluminophosphate molecular sieves (MeAPO-*n*) is a useful tool for the modification of the properties of such materials, enabling the study of their crystallization process[18,19] and possible applications.[20,21] However, the effect of transition metals on the crystallization process of AlPO-5 *via* the ionothermal and H_3PO_3-containing route is still unknown, and hence it is worth further exploring.

In this work, the ionothermal crystallization of FeAPO-5 using phosphorous acid (H_3PO_3) as the phosphorus source is

[a] *School of Chemical Sciences, Universiti Sains Malaysia, 11800 USM, Penang, Malaysia. E-mail: epng@usm.my; Tel: +6046534021*
[b] *Laboratoire Catalyse & Spectrochimie, CNRS-ENSICAEN, Université de Caen, France*
[c] *Institute of Biological Sciences, Faculty of Science, University of Malaya, Kuala Lumpur, Malaysia*

reported. The formation process of FeAPO-5 during the ionothermal synthesis was monitored by microscopic and spectroscopic methods. A possible mechanism for the growth of FeAPO-5 crystals was proposed based on the experimental results.

2. Experimental

Synthesis of [bdmim]Cl

The [bdmim]Cl ionic molten salt was prepared by using the modified synthesis procedure from ref. 22: 1,2-dimethylimidazole (45.00 g, 96%, Merck) was dissolved in ethanol (40 mL, 99.7%, QRëC) in a 250 mL round bottom flask. Benzyl chloride (86 mL, 99%, Merck) was then added to the mixture. The resulting solution was refluxed at 100 °C for 6 h. The round bottom flask was cooled down and placed in an ice bath to allow white crystals to precipitate out (Scheme 1). The white crystals were purified and washed with acetone prior to drying in an oven at 100 °C overnight. The pure ionic molten salt was kept in a tight polypropylene bottle and stored in a desiccator. A product yield of 86.4% was obtained. ^{1}H NMR (400 MHz, ppm, D_2O) appeared as follows: δ = 2.48 (3H, imidazole N–C(C*H*$_3$)–N), 3.70 (3H, imidazole N–C*H*$_3$), 4.70 (2H, imidazole N–C*H*$_2$–C_6H_5), 7.22 (1H, imidazole N–C*H*═CH–N), 7.24 (1H, imidazole N–CH═C*H*–N) and 7.28–7.41 (5H, phenyl). FT-IR (KBr disk, cm^{-1}): 1036 (imidazolium, C–N), 1452 and 1638 (aromatic C═C), 1530 (imidazolium, C═N), 3497 (O–H stretching). Anal. calcd for $C_{12}H_{15}N_2Cl$: C, 64.72%; H, 6.79%; N, 12.58%; Cl, 15.92%; found: C, 65.03%; H, 6.66%; N, 11.55%; Cl, 16.77%.

Ionothermal synthesis of FeAPO-5

The synthesis of FeAPO-5 was carried out in a 50 mL Teflon-lined stainless steel autoclave. Prior to the synthesis, H_3PO_3 (0.421 g, 85%, Sigma-Aldrich) and $FeCl_3{\cdot}6H_2O$ (0.0178 g, 98%, Merck) were first dissolved in distilled water (0.0743 g). Aluminum isopropoxide (0.416 g, 98%, Sigma-Aldrich) and [bdmim]Cl ionic molten salt (8.89 g) were then introduced into the mixture and the autoclave was sealed prior to heating at 170 °C for 10 min. The final gel molar composition of FeAPO-5 was IL : Al : P : Fe : H_2O = 80 : 2 : 6 : 0.13 : 11.5. The reactor vessel was cooled down and the solid product was washed carefully with double distilled water before drying at 80 °C overnight. A similar procedure was also adopted for the solid products after different crystallization time periods (20 min, 1 day, 3 days and 5 days).

Characterization

Powder XRD patterns were recorded on a PANalytical X'Pert PRO diffractometer with Cu K_α radiation (λ = 0.15418 nm, 40 mA, 45 kV, a step size of 0.02° and a scan speed of 0.2° min^{-1}). The morphology of the powder samples was analyzed by using a Leo Supra 50VP field emission scanning electron microscope (FESEM) operating at 30 kV. The FTIR spectra of the samples were obtained using the KBr pellet technique in the range of 400–2800 cm^{-1}. The UV-vis spectra of the solids were measured in the spectral range of 200–500 nm using a Varian Cary® 100 UV-vis-NIR spectrophotometer. ^{27}Al and ^{31}P solid-state MAS NMR measurements were conducted on a Bruker Ultrashield 500 spectrometer at MAS frequencies between 5 and 15 kHz. The ^{27}Al and ^{31}P MAS NMR spectra were obtained with 8000 scans by single-pulse excitation using π/12 (0.6 μs) and π/2 (3 μs) pulses, respectively. Similarly, ^{13}C solid-state CP/MAS NMR measurements were conducted too (spinning speed of 14.5 kHz at a magnetic field of 9.4 T with a resonance frequency of 104.26 MHz using the single-pulse mode at 1 ms contact time).

3. Results and discussion

XRD analysis

Fig. 1 shows the XRD patterns of the products. The solid was found to be amorphous after 10 minutes of treatment as indicated by the absence of reflections in the X-ray diffractogram. Several diffraction peaks at 2θ = 12.98°, 25.96°, 29.09° and 34.17° appear after 20 min. These peaks are assigned to FeNKX-2, an aluminophosphite intermediate.[8] As compared to NKX-2 aluminophosphite (Fig. 1f), the peaks are slightly right-shifted due to the incorporation of Fe^{3+} into the NKX-2 framework. It is worth mentioning here that the incorporation of Fe^{3+} has shortened the crystallization time of NKX-2 to 20 min, which is much faster than those observed for the products prepared using ionothermal (170 °C, 5 h) and hydrothermal (195 °C, 6 days) methods reported previously.[8,17] An attempt to use $Fe(NO_3)_3$ instead of $FeCl_3$ as the Fe^{3+} source was also made in order to study the effect of the salt used, and fully crystalline FeNKX-2 was obtained within similar time.

After 1 day of heating, several small peaks at 2θ = 7.46°, 19.77°, 21.15° and 22.47°, which correspond to FeAPO-5,

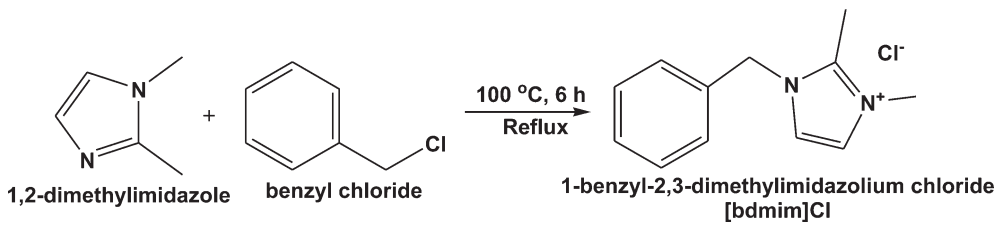

Scheme 1 Synthesis of [bdmim]Cl ionic molten salt.

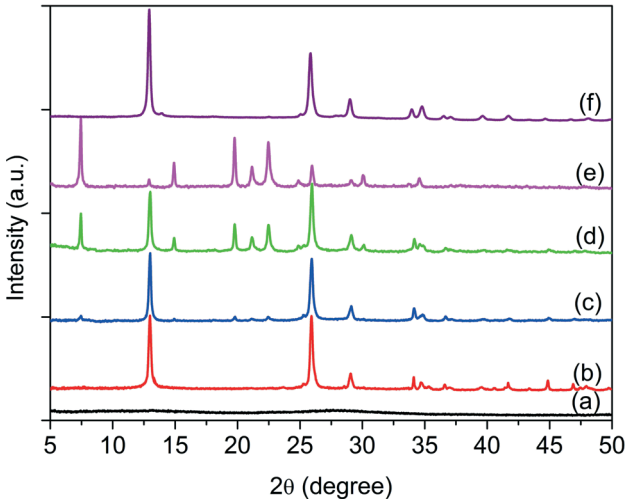

Fig. 1 XRD patterns of solid products after (a) 10 min, (b) 20 min, (c) 1 day, (d) 3 days and (e) 5 days of ionothermal synthesis. The XRD pattern of pure NKX-2 aluminophosphite is shown in (f).

emerge. After extending the crystallization time up to 3 days, the FeAPO-5 phase becomes dominant and full transformation of the FeNKX-2 ferroaluminophosphite intermediate into FeAPO-5 ferroaluminophosphate was achieved within 5 days.

The synthesis was also carried out without adding the $FeCl_3$ salt. It was observed that the crystallization time for obtaining the NKX-2 aluminophosphite intermediate was extended to 3 h and this phase was stable with further increase of the heating time, *i.e.* the AlPO-5 crystalline phase was not detected even after 20 days of ionothermal treatment. An attempt to use H_3PO_4 instead of H_3PO_3 for the synthesis of FeAPO-5 was also made, and no trace of FeNKX-2 was observed under the same gel composition and crystallization conditions.

SEM microscopy study

The crystallization of FeAPO-5 in an ionic liquid with H_3PO_3 was monitored by SEM analysis. The initial amorphous solid material (10 min) is composed of nanoparticles (*ca.* 120 nm) with irregular shapes (Fig. 2a and b). The nanoparticles tend to agglomerate to form bulk entities with micrometer sizes. The morphology of the bulk solid changes after 20 min; the FeNKX-2 crystals with more pronounced structural features start to form (Fig. 2c and d). As shown in Fig. 2c, the FeNKX-2 crystals (size of *ca.* 0.6–2.5 μm) show a novel rounded rectangle-like morphology with a rough surface, which is different from the hydrothermally and ionothermally synthesized NKX-2 crystals.[8,17] This could be due to the absence of fluoride ions and the use of a different ionic liquid ([bdmim]Cl) as a solvent and a template during the ionothermal synthesis.

After 1 day of crystallization, the rounded rectangle-like FeNKX-2 crystals containing FeAPO-5 as a minor phase agglomerate with each other and form big spherical particles

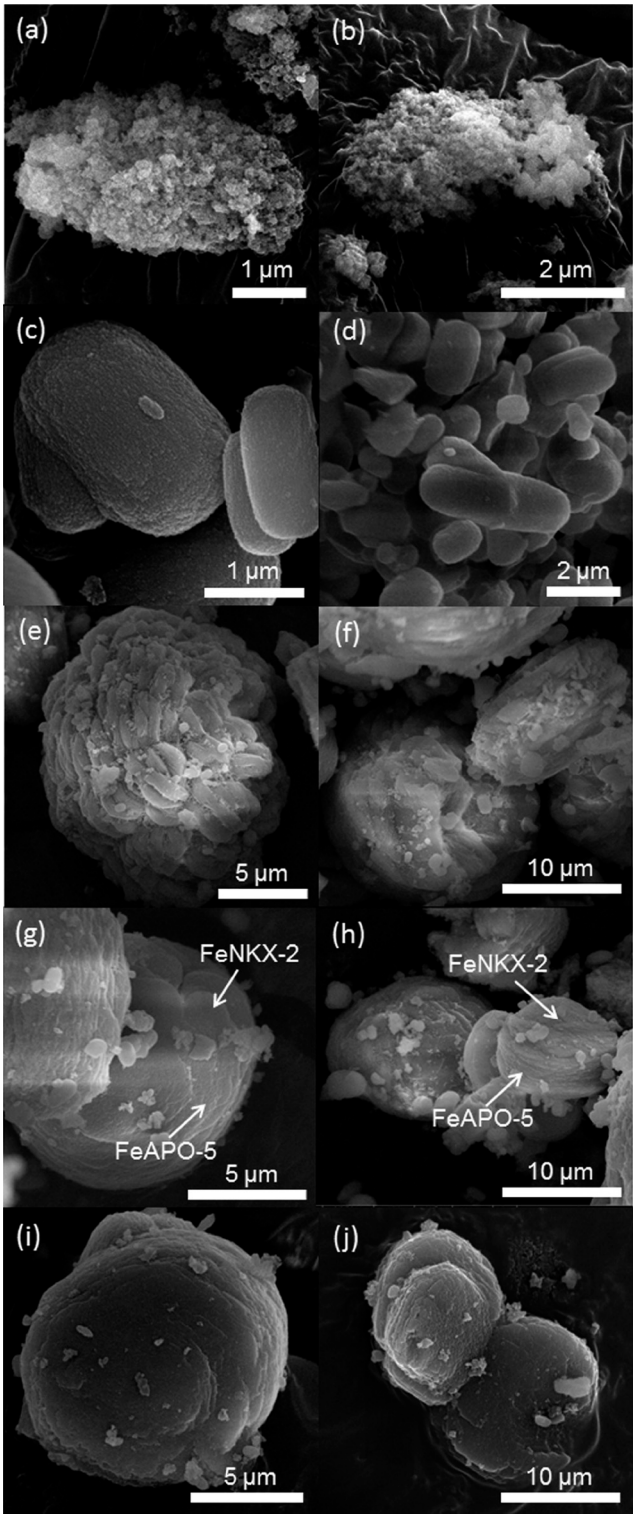

Fig. 2 SEM images of solid products after (a, b) 10 min, (c, d) 20 min, (e, f) 1 day, (g, h) 3 days and (i, j) 5 days of ionothermal synthesis at different magnifications.

with a size of *ca.* 13.8 μm (Fig. 2e and f). With prolongation of the crystallization time up to 3 days, big spherical particles (*ca.* 11.5 μm) containing both the FeNKX-2 intermediate and FeAPO-5 crystalline solids are observed (Fig. 2g and h). As is

shown, these FeNKX-2 intermediate crystals slowly dissolve in the ionic liquid, and FeNKX-2 crystals with a smooth surface and rectangle-like morphology appear and become embedded within the big spherical entities (Fig. 2g and h). Furthermore, the FeAPO-5 phase is also observed in the big spherical solid, arranging as stacking layered hexagonal thin flakes. Thus, the change in the morphology of the crystals reveals that phase transformation takes place in the ionic liquid medium, which is in line with the XRD observation (Fig. 1d). The FeNKX-2 phase is completely consumed and pure FeAPO-5 crystals are formed after 5 days of ionothermal treatment (Fig. 2i and j). As can be seen in the micrograph, the resulting crystals have sizes of about 13.0 μm with stacking layered hexagonal thin flakes growing in rounded hexagonal-shaped crystals.

ICP-AES elemental analysis

The elemental compositions of the solids measured by ICP-AES are shown in Table 1. The analysis shows that Fe^{3+} cations participate in the early stage of the crystallization process. Initially, 1.53 mol% Fe is found in the powder solid, and the Fe content keeps increasing with increasing ionothermal synthesis time. After 20 min, a P/(Al + Fe) ratio of 1.51 is obtained when the FeNKX-2 solid is formed which corresponds to the P/Al ratio of pure NKX-2 (1.50).[17] The amount of Fe^{3+} incorporated into the crystalline framework continues to increase where 3.23 mol% Fe is recorded for the FeNKX-2/FeAPO-5 mixture after 3 days. After 5 days, pure FeAPO-5 with a P/(Al + Fe) ratio of 0.99 is measured. The final FeAPO-5 contains 3.39 mol% Fe, which is higher than the amount of Fe incorporated into the AFI framework using a hydrothermal approach (3.0 mol% Fe).[23]

UV-visible spectroscopy analysis

The incorporation of Fe^{3+} into the solid entities was further investigated by UV-visible spectroscopy. Initially, the amorphous sample which underwent 10 min of heating exhibits two bands at 218 nm and 260 nm (Fig. 3a). The sharp absorption band at 218 nm is attributed to finely dispersed Fe^{3+} in the framework position, whereas the band at 260 nm is due to the ligand-to-metal charge transfer (LMCT) band of Fe^{3+} in tetrahedral positions.[24] The peak intensities increase significantly as FeNKX-2 is formed after 20 min (Fig. 3b). Thus, the

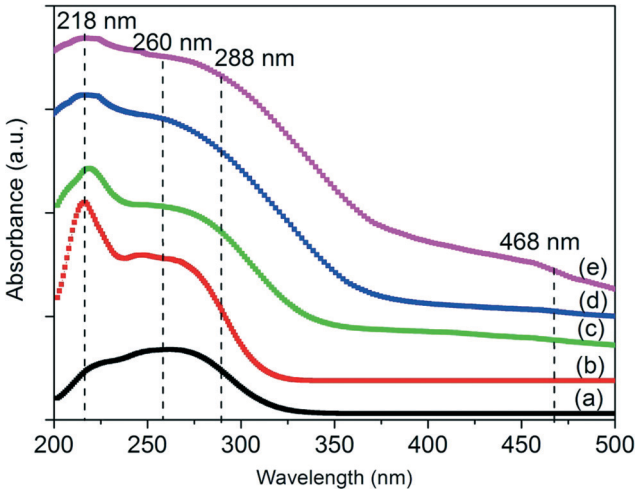

Fig. 3 UV-visible spectra of solid products after (a) 10 min, (b) 20 min, (c) 1 day, (d) 3 days and (e) 5 days of ionothermal synthesis.

UV-vis spectroscopy study reveals that Fe^{3+} participates actively in the construction of the NKX-2 framework. Upon increasing the heating time, the band at 218 nm slowly disappears. These iron species are gradually converted to tetrahedral framework iron species, where a strong shoulder band at 288 nm slowly appears (Fig. 3e). Furthermore, a weak band at 468 nm also emerges and it can be attributed to the octahedral Fe^{3+} species.[25]

Infrared spectroscopy analysis

A complementary FTIR spectroscopy study was performed to monitor the crystallization kinetic process of the solid. As can be seen in Fig. 4a, only several IR bands are observed for the amorphous sample (10 min) at 2432, 1096, 1017 and 625 cm^{-1} which correspond to the P–H stretching mode of HPO_3^{2-} and the symmetrical vibrations of PO_2^-, P–O and TO_4 (T = Al, P or Fe), respectively. After ionothermal heating for 20 min, the solid exhibited an IR spectrum identical to that of pure NKX-2 where the above described bands are slightly shifted to 2469, 1217, 1139, 1036, 588 and 549 cm^{-1}.[17] This indicates that Fe is incorporated into the NKX-2 material. No peak is observed at 1400–1550 cm^{-1} indicating that no $[bdmim]^+$ cation is chemically bound to the amorphous and crystalline FeNKX-2 solids (inset of Fig. 4a and b).

Table 1 Framework compositions of the solid samples

Phase(s)	Crystallization time	Atomic ratios			P/(Al + Fe) ratio	Fe/(Al + P + Fe) ratio (mol%)
		Al	P	Fe		
Amorphous	10 min	0.611	1.000	0.025	1.57	1.53
FeNKX-2	20 min	0.619	1.000	0.038	1.52	2.29
FeNKX-2, FeAPO-5*	1 day	0.670	1.000	0.051	1.39	2.96
FeNKX-2, FeAPO-5	3 days	0.826	1.000	0.061	1.13	3.23
FeAPO-5	5 days	0.938	1.000	0.068	0.99	3.39

*Trace amount.

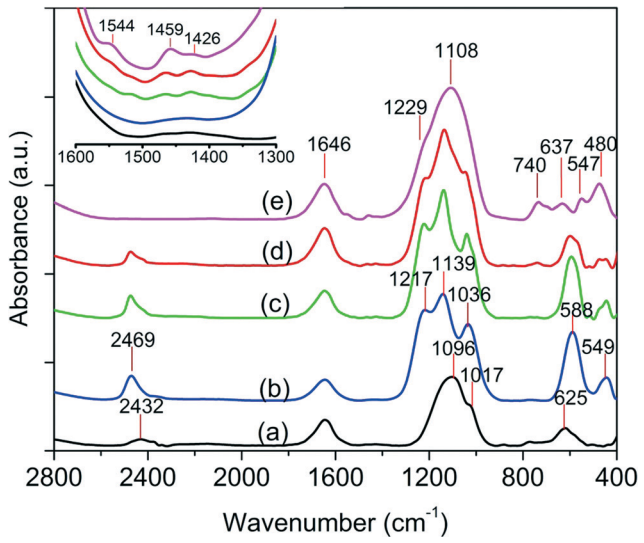

Fig. 4 IR spectra of solid products after (a) 10 min, (b) 20 min, (c) 1 day, (d) 3 days and (e) 5 days of ionothermal synthesis.

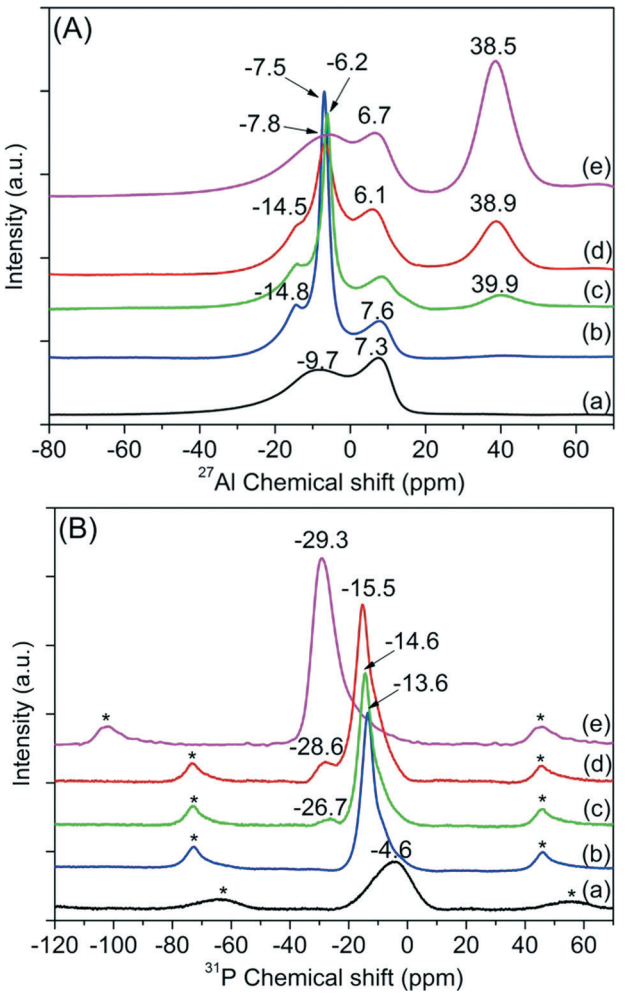

Fig. 5 (A) ^{27}Al and (B) ^{31}P MAS NMR spectra of solid products after (a) 10 min, (b) 20 min, (c) 1 day, (d) 3 days and (e) 5 days of ionothermal synthesis.

The IR spectra especially at the fingerprint region (1300–400 cm^{-1}) change with further heating. The IR signals at 1426, 1459 and 1544 cm^{-1}, which correspond to the $[bdmim]^+$ cation, slowly appear (inset of Fig. 4c–e). Furthermore, the IR bands at 1000–1250 cm^{-1} change slowly and a strong band with shoulders at 1108 and 1229 cm^{-1}, corresponding to external linkage asymmetrical stretching and internal T–O–T (T = Al, P, Fe) tetrahedral asymmetrical stretching, respectively, is detected after 5 days. Furthermore, the signals at 1036 and 2469 cm^{-1} which are attributed to the P–H stretching and P–H deformation modes of HPO_3^{2-}, respectively, slowly disappear with heating time. Concurrently, four characteristic bands of the AFI framework (480, 547, 637 and 740 cm^{-1})[26] start to appear after 3 days, showing that phase transformation to the AFI framework structure is taking place, which agrees with the XRD and SEM results. The four characteristic bands of the AFI framework become more profound as heating of the solid is further prolonged to 5 days. The solid exhibits an IR spectral pattern similar to that of the pure AFI phase indicating that fully crystalline FeAPO-5 has been obtained (Fig. 4e).

^{31}P and ^{27}Al MAS NMR spectroscopy analyses

The evolution of the crystalline structure during the amorphous–intermediate–crystal transformation was monitored as a function of time by ^{27}Al and ^{31}P MAS NMR spectroscopy. Fig. 5 shows the ^{27}Al and ^{31}P MAS NMR spectra of the solid samples after ionothermal treatment for various times. Initially, two broad signals at −9.7 and 7.3 ppm in the ^{27}Al MAS NMR spectrum are observed which are assigned to the octahedral and pentahedral aluminum species due to $Al(MO)_4(OH_2)_2$ and $Al(MO)_4(OH_2)$ (M = P, Fe), respectively (Fig. 5A(a)).[27] No signals are detected at 1.7 and 61.5 ppm indicating that aluminum isopropoxide has completely dissolved and reacted in the ionic liquid after 10 min.[28,29] When the solid is heated for 20 min, the peak at −9.7 ppm splits into two peaks at −14.8 and −7.5 ppm (Fig. 5A(b)). The first intense peak at −14.8 ppm is due to octahedral AlO_6 species, which share three Al–O corners with three HPO_3^{2-} tetrahedra and three Al–O corners with one adjacent AlO_6 octahedron.[8] The second band at −7.5 ppm can be assigned to $[Al_2(HPO_3)_3]$ species, which are the basic building units of the FeNKX-2 material. These two signals, however, slowly decrease and shift downfield (−14.8 → −14.5 ppm and −7.5 → −6.2 ppm) with increasing crystallization time (Fig. 5A(c and d)). This indicates that the matrix suffers from a loss of lattice periodicity due to distorted chemical bonds in Al sites and the presence of the AFI crystalline phase. In addition, a new band emerges at 39.9 ppm which is attributed to the tetrahedral Al species in the AFI-type framework.[27] The pentahedral Al signal, on the other hand, is shifted from 7.6 ppm to 6.1 ppm. The changes in the ^{27}Al MAS NMR spectra are in good agreement with the changes observed through XRD and SEM analyses at the macroscopic

level. After 5 days, the peaks in the range of −20 to 0 ppm are completely disrupted, producing a broad band at −7.8 ppm. The signal at 38.9 ppm shifts gradually to 38.5 ppm and becomes dominant, which suggests that the tetrahedral Al is in a different chemical environment in the fully crystalline FeAPO-5 sample (Fig. 5A(e)). In addition, a significant chemical shift of tetrahedrally coordinated Al is also observed when Fe^{3+} is incorporated into the framework of AlPO-5; the chemical shift of as-synthesized AlPO-5 is 36.0 ppm.[30]

The ^{31}P MAS NMR spectra of the samples are shown in Fig. 5B. A broad signal at −4.6 ppm was detected in the sample at the beginning of the ionothermal synthesis (10 min) (Fig. 5B(a)). This peak, which is assigned to $P(OH)_2(OM)_2$ (M = Al, Fe), is relatively broad and not well resolved. This indicates a disordered environment around the P site for the sample, which is in agreement with the amorphous character of the XRD pattern (see Fig. 1). Upon ionothermal heating for 20 min, these local environments evolve to become $P(H)(OAl_{Oct})_3$ tetrahedral species where an upfield shift to −13.6 ppm is recorded (Fig. 5B(b)). The signal is sharp due to the symmetry of the tetrahedral phosphite species in FeNKX-2. The peak in the region from 0 to −19.0 ppm can also be assigned to the lower condensation degree of phosphorus species, which is in line with the IR spectroscopy data for the FeNKX-2 samples proving the existence of the P–H bond.[31,32] After 1 day of crystallization, the peak at −13.6 ppm is shifted to −14.6 ppm and is broadened as well. This is due to the distortion of the FeNKX-2 structure, in addition to the change of the chemical environment of P in the matrix during the ionothermal process. A small peak at −26.7 ppm is also observed which can be ascribed to P sites connected to both tetrahedral and octahedral Al sites, which are present in the AFI crystalline solid.[27] Thus, the NMR study reveals that phase transformation from FeNKX-2 to FeAPO-5 takes place. The peak shifting and broadening remain and the intensity of the peak at −28.6 ppm, which corresponds to tetrahedral P species in FeAPO-5, increases after 3 days. After 5 days of heating, a single peak at −29.3 ppm indicating the complete transformation to FeAPO-5 is detected.[22] As is shown, the peak is sharp and this reveals that only one distinguishable type of tetrahedral phosphorus is present in the AFI structure.

Fe^{3+} substitution in the AlPO-5 framework can also be proven by ^{31}P MAS NMR spectroscopy besides observing the low-field chemical shift of the peak of tetrahedrally coordinated Al in the ^{27}Al MAS NMR spectrum (Fig. 5A(e)).[33–35] Due to the strong dipolar coupling between ^{31}P and paramagnetic Fe^{3+} species, intense sidebands are usually observed in the MAS spectra. It can be seen that intense sidebands are observed even at the very early stage of ionothermal synthesis (Fig. 5). Thus, the ^{31}P MAS NMR spectroscopy data are in agreement with those of UV-vis spectroscopy, *i.e.* Fe^{3+} participates actively in the crystallization process of the FeAPO material.

^{13}C MAS NMR spectroscopy analysis

The $[bdmim]^+$ cations confined in the micropores of the FeNKX-2 and FeAPO-5 samples were studied using ^{13}C MAS NMR spectroscopy. The results reveal that no carbon peaks are detected in the solid after 20 min of ionothermal heating, indicating that no $[bdmim]^+$ cation is confined in the micropores of the FeNKX-2 sample (Fig. 6a). Thus, it can be concluded that $[bdmim]^+$ cations do not play the role of pore-filling agents during the formation of the FeNKX-2 framework structure. As the heating time was extended to 3 days, where the AFI phase started to form (Fig. 1), some small signals corresponding to $[bdmim]^+$ cations started to appear (Fig. 6b). The signals at 128.68 and 123.31 ppm are assigned to the C5 and C4 atoms in the imidazole ring, and the resonance peaks at 36.65 and 9.41 ppm represent the C8 and C7 atoms of alkyl groups attached to the imidazole ring (inset of Fig. 6). Thus, the ^{13}C NMR results imply that $[bdmim]^+$ cations start to be confined in the micropores of the FeAPO-5 sample, which is consistent with the IR results (inset of Fig. 4). The ^{13}C signals of $[bdmim]^+$ occluded in the AFI framework become profound as heating of the solid is further extended to 5 days, and fully crystalline FeAPO-5 is formed (Fig. 6c). As is shown, all the signals are present thus indicating that the $[bdmim]^+$ molecules are preserved upon occlusion in the AFI crystals. Thus, the NMR spectroscopy data confirm that the $[bdmim]^+$ cations act as pore-filling agents which direct the formation of FeAPO-5 during the ionothermal treatment.

Growth mechanism of FeAPO-5

Classically, the AFI-type framework is templated by amines or quaternary ammonium salts under hydrothermal conditions using H_3PO_4 as a phosphorus source.[36] H_3PO_3 is generally described with the structural formula $HPO(OH)_2$ in which this species exists in equilibrium with a $P(OH)_3$ tautomer. Because of the rapid interconversion, these tautomers alter the charge of P species in the NKX-2 and AFI frameworks ($P^{3+} \leftrightarrow P^{5+}$). Thus, the use of H_3PO_3 enables exploration of the

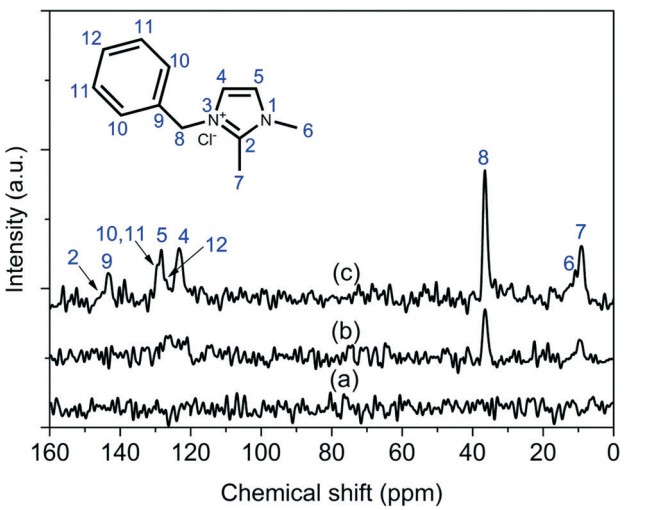

Fig. 6 ^{13}C MAS NMR spectra of solid products after (a) 10 min, (b) 3 days and (c) 5 days of ionothermal synthesis.

metastable intermediate phase with a novel open-framework crystalline phase and unique framework properties. H_3PO_3 as a phosphorus source, however, is seldom used in the synthesis of AlPO-*n* materials neither in hydrothermal[8,9,12] nor in ionothermal[17] pathways. On the other hand, it was reported that the dibasic H_3PO_3 acid (pK_{a1} = 1.80, pK_{a2} = 6.15) has stronger acidity compared to H_3PO_4 (pK_{a1} = 2.12, pK_{a2} = 7.21, pK_{a3} = 12.67), and its acidity and the oxidation state of P species also govern the selectivity to the crystalline phase product during the crystallization process.[9,10]

The ionothermal synthesis pathway of FeAPO-5 *via* the H_3PO_3-containing route is shown in Fig. 7. During the initial 10 min of heating, the process involves the mixing of raw aluminum isopropoxide, H_3PO_3 and $FeCl_3$ in the [bdmim]Cl ionic liquid, followed by successive dissolution (Stage I). As revealed by ^{27}Al MAS NMR, aluminum isopropoxide completely hydrolyzes within 10 min in the polar [bdmim]Cl ionic liquid, and then further reacts with H_3PO_3 to form $Al(MO)_4(OH_2)_2$ (M = P, Fe) monomers and oligomers (Stage II). These intermediates are composed of H–P–O, P–O–Al, P–O–Fe and Al–O–Fe units which are present, along with free phosphite and Fe^{3+} species as well, in the mixture.

In the absence of Fe^{3+}, the intermediates slowly undergo reorganization and the NKX-2 structure is formed after 5 h of ionothermal heating or 6 days of hydrothermal treatment. The crystallization rate, however, is significantly enhanced where the construction of the NKX-2 framework structure is achieved merely in 20 min in the presence of Fe^{3+} under ionothermal heating (Stage III). During the crystallization process, Fe^{3+} species actively participate in the isomorphous incorporation in the NKX-2 framework. After 20 min of ionothermal synthesis, 2.29 mol% Fe is incorporated into the framework of NKX-2. On the other hand, the Al species existing in FeNKX-2 are in octahedral form, and it is connected to HPO_3^{2-} tetrahedra and AlO_6 octahedra; whereas, the P species appear in the form of $P(H)(OAl_{Oct})_3$ tetrahedral species. No [bdmim]Cl is confined in the pores of FeNKX-2 as revealed by FTIR spectroscopy, indicating that the $[bdmim]^+$ cation does not function as a pore-filling agent during the construction of the FeNKX-2 crystalline structure. As can be seen in the SEM image (Fig. 2b), the FeNKX-2 crystals (*ca.* 1.4–2.5 μm) exhibit a novel rounded rectangle-like morphology with a rough surface.

After 1 day of ionothermal treatment, the FeNKX-2 crystals agglomerated with each other, forming big spherical particles (*ca.* 13.8 μm) (Stage IV). In addition, the peaks (1544, 1463 and 1425 cm^{-1}) corresponding to $[bdmim]^+$ appear in the IR spectrum of the solid sample (Fig. 4d). Thus, this indicates that the inorganic monomers and oligomers slowly enfold the $[bdmim]^+$ cations through van der Waals interactions to form AFI micropores.[27] This observation is supported by the XRD study where the beginning of phase transformation to

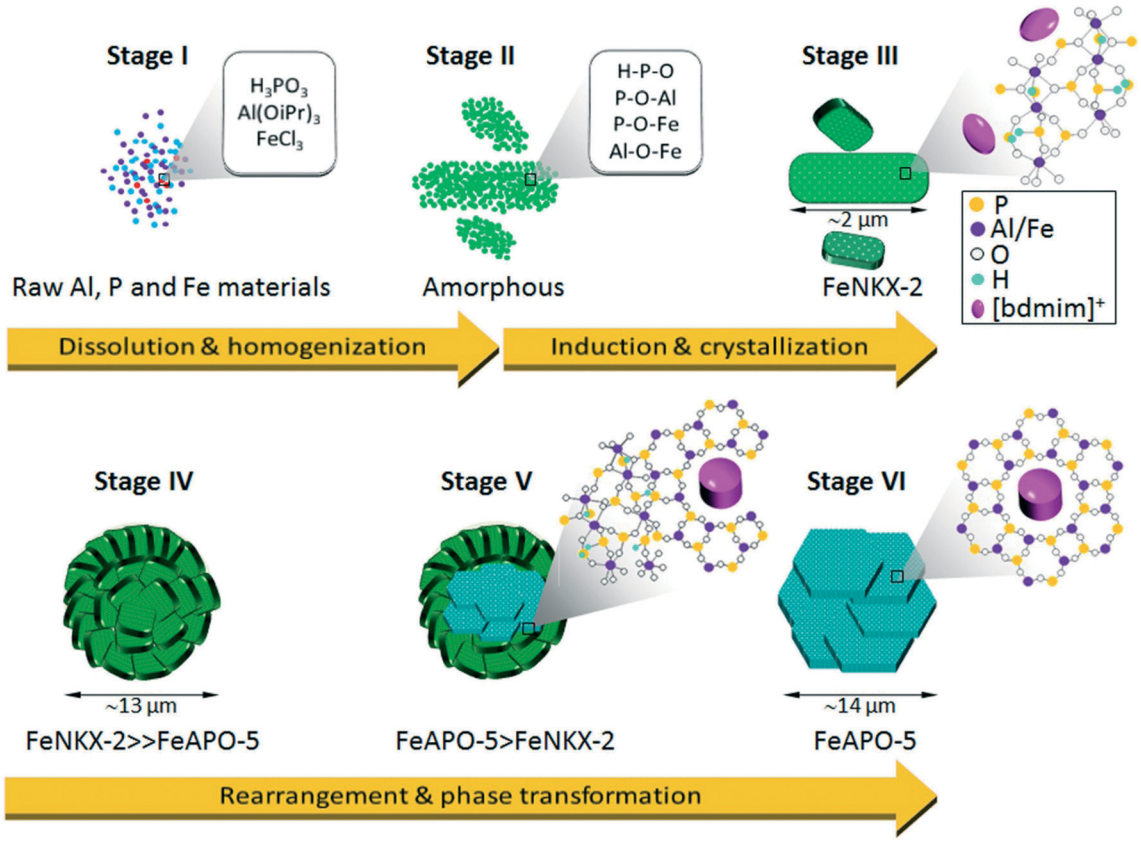

Fig. 7 The ionothermal crystallization pathway of FeAPO-5 through the H_3PO_3-containing route.

the AFI crystalline phase is revealed. During this period of time, the iron species in FeNKX-2 are gradually converted to tetrahedral framework iron species. Furthermore, the aluminum species, which is octahedrally coordinated in FeNKX-2, is partially converted into tetrahedrally coordinated Al in the AFI framework. The phosphorus species are present in metaphosphite units where slightly distorted HPO_3^{2-} tetrahedral units are slowly converted to PO_4^{3-} tetrahedral units *via* changing the oxidation state of P^{3+} to P^{5+}.

From these results, we believe that the transformation of pseudo-tetrahedral HPO_3^{2-} species (−7.7 kcal mol^{-1}) to tetrahedral PO_4^{3-} species (−12.0 kcal mol^{-1}) requires high activation energy.[37,38] This is the reason why no transformation of phosphorus species ($P^{3+} \rightarrow P^{5+}$) was observed in the absence of Fe^{3+}. However, the activation energy of the transformation of pseudo-tetrahedral HPO_3^{2-} species to tetrahedral PO_4^{3-} species is significantly reduced with the addition of Fe^{3+}. The UV-vis spectroscopy data reveal that Fe^{3+} initially exists in the form of a ligand-to-metal charge transfer (LMCT) complex. This tetrahedral Fe^{3+} species can act as an intermediary electron-transfer medium allowing the change of the oxidation state from P^{3+} to P^{5+}, and the tetrahedral Fe^{3+} species can even take part in the isomorphous incorporation in both the NKX-2 and AFI frameworks.

During the FeAPO-5 nucleation process, the dissolved FeNKX-2 particles aggregate and form nuclei, which serve as the crystallization centre of FeAPO-5. Following the rapid nucleation process, the FeAPO-5 nuclei grow larger with time and form the AFI molecular sieve structure. The phase transformation continues to take place after 3 days (Stage V). This phenomenon can be proven by the XRD study where the peaks corresponding to the AFI phase become dominant (Fig. 1c and d). Furthermore, the IR peak intensity of $[bdmim]^+$ becomes stronger (Fig. 4c and d) indicating that more and more $[bdmim]^+$ molecules are interacting and confined inside the micropores of FeAPO-5. The pseudo-tetrahedral HPO_3^{2-} species still co-exist with the tetrahedral PO_4^{3-} species in the FeNKX-2/FeAPO-5 intermediates. This transformation thus may lead to the formation of highly strained tetrahedral T-atom sites present in the framework and play the key role in the formation of FeAPO-5. Furthermore, the terminal P–H bond of HPO_3^{2-} slowly disappears with heating time *via* its tautomerism involving shifts of H between O and P.

After 5 days of heating, pure FeAPO-5 is formed. The size of the crystals remains almost constant (*ca.* 14 μm) during the whole phase transformation process which can be explained by the slow and controlled oxidation–reduction chemistry reaction ($P^{3+} \rightarrow P^{5+}$) that favours the procedure for retarding the crystal growth of FeAPO-5 molecular sieves (Stage VI). At this stage, the structure of crystalline FeAPO-5 consists of an ordered covalent network involving tetrahedral $[PO_{4/2}]^+$, $[AlO_{4/2}]^-$ and $[FeO_{4/2}]^-$ units. Furthermore, the $[bdmim]^+$ cation is completely enfolded and occluded into the channels of the FeAlPO-5 crystals based on FTIR spectroscopy data.[27]

4. Conclusions

A detailed investigation of the ionothermal synthesis of FeAPO-5 molecular sieves in the presence of H_3PO_3 has been reported. The results show that initially raw chemicals dissolve rapidly in the [bdmim]Cl polar ionic liquid. By adding the Fe^{3+} salt to the reaction mixture, the FeNKX-2 intermediate is crystallized within 20 min instead of 3 h of heating. The study also reveals that the $[bdmim]^+$ cation does not function as a pore-filling agent during the construction of the FeNKX-2 crystalline structure. The phase transformation from FeNKX-2 to FeAPO-5 starts after 1 day of heating. During this stage, the tetrahedral Fe^{3+} species was found to not only participate in the construction of the NKX-2/AFI framework but also act as an intermediary electron-transfer medium. As a result, the oxidation of phosphite (P^{3+}) to phosphate (P^{5+}) was enhanced resulting in the fast release of phosphorus nutrients (P^{5+}) that are required for the crystallization and growth of FeAPO-5. Furthermore, confinement of $[bdmim]^+$ cations by the anionic ferroaluminophosphate intermediate is also observed along the phase transformation process. Fully crystalline FeAPO-5 was obtained after 5 days of ionothermal synthesis.

Thus, the use of ionic liquids as dual solvents and templates in combination with H_3PO_3 as an alternative phosphorus source offers the possibility of preparing FeAPO microporous materials *via* the phase transformation method. The highly porous FeAPO samples with insufficient thermal stability are not used in catalysis yet. However, considerable efforts in improving the thermal stability of the FeAPO samples to explore further their catalytic properties are in progress.

Acknowledgements

Financial support from RUI (1001/PKIMIA/811264) and USM Short-term (304/PKIMIA/6313047) Grants is acknowledged. J. P. Ghoy would also like to thank the MyBrain and USM Fellowship for the scholarship provided.

References

1 S. Henninger, F. Schmidt and H.-M. Henning, *Appl. Therm. Eng.*, 2010, **30**, 1692–1702.
2 E. P. Ng, L. Delmotte and S. Mintova, *ChemSusChem*, 2009, **2**, 255–260.
3 F. Adam, J.-T. Wong and E.-P. Ng, *Chem. Eng. J.*, 2013, **214**, 63–67.
4 E. Hu, Y. L. W. Huang, Q. Yan, D. Liu and Z. Lai, *Microporous Mesoporous Mater.*, 2009, **126**, 81–86.
5 E. Leite, T. Babeva, E.-P. Ng, V. Toal, S. Mintova and I. Naydenova, *J. Phys. Chem. C*, 2010, **114**, 16767–16775.
6 M. K. Song and K. T. No, *Int. J. Hydrogen Energy*, 2009, **34**, 2325–2328.
7 L. Tosheva, E.-P. Ng, S. Mintova, M. Holzl, T. H. Metzger and A. M. Doyle, *Chem. Mater.*, 2008, **20**, 5721–5726.
8 N. Li, Y. Ma, S. Xiang and N. Guan, *Chem. Mater.*, 2006, **18**, 975–980.

9 W. Kong, W. Dai, N. Li, N. Guan and S. Xiang, *J. Mol. Catal. A: Chem.*, 2009, **308**, 127–133.
10 P. W. Atkins, T. Overton, J. P. Rourke, M. Weller and F. A. Armstrong, *Inorganic Chemistry*, Oxford University Press, UK, Fifth edn., 2010.
11 H. Chen, R. Chao, B. Na, N. Li, S. Xiang and N. Guan, *Chin. J. Catal.*, 2007, **28**, 501–503.
12 N. Li, G. Cao and S. Xiang, *Stud. Surf. Sci. Catal.*, 2004, **154**, 1001–1006.
13 E. R. Cooper, C. D. Andrews, P. S. Wheatley, P. B. Webb, P. Wormald and R. E. Morris, *Nature*, 2004, **430**, 1012–1016.
14 E. R. Parnham and R. E. Morris, *Acc. Chem. Res.*, 2007, **40**, 1005–1013.
15 T. Laher and C. Hussey, *Inorg. Chem.*, 1983, **22**, 3247–3251.
16 E.-P. Ng, S. S. Sekhon and S. Mintova, *Chem. Commun.*, 2009, 1661–1663.
17 Y. Shi, X. Zhang, L. Wang and G. Liu, *Mater. Lett.*, 2014, **124**, 212–214.
18 J. Kornatowski, G. Zadrozna, M. Rozwadowski, B. Zibrowius, F. Marlow and J. A. Lercher, *Chem. Mater.*, 2001, **13**, 4447–4456.
19 M. Dong, G. Wang, Z. Qin, J. Wang, T. Liu, S. Yuan and H. Jiao, *J. Phys. Chem. A*, 2007, **111**, 1515–1522.
20 L. Qi, X. Qi, J. Wang and L. Zheng, *Catal. Commun.*, 2011, **16**, 225–228.
21 F. Wang, L. Liang, J. Ma and J. Sun, *Mater. Lett.*, 2013, **111**, 201–203.
22 D. Y. Khoo, W.-M. Kok, R. R. Mukti, S. Mintova and E.-P. Ng, *Solid State Sci.*, 2013, **25**, 63–69.
23 A. Bruckner, U. Lohse and H. Mehner, *Microporous Mesoporous Mater.*, 1998, **20**, 207–215.
24 W. Wei, J. A. Moulijn and G. Mul, *Microporous Mesoporous Mater.*, 2008, **112**, 193–201.
25 A. Kostapapas, S. L. Suib, R. W. Coughlin and M. L. Occelli, in *Zeolites: Facts, Figures, Future: Facts, Figures, Future*, ed. P. A. Jacobs and R. A. van Santen, Elsevier Science Publishing Company Inc., Netherlands, 1990, pp. 399–409.
26 D. Y. Khoo, H. Awala, S. Mintova and E.-P. Ng, *Microporous Mesoporous Mater.*, 2014, **194**, 200–207.
27 E. P. Ng, L. Itani, S. S. Sekhon and S. Mintova, *Chem. – Eur. J.*, 2010, **16**, 12890–12897.
28 N. Y. Turova, V. Kozunov, A. Yanovskii, N. Bokii, Y. T. Struchkov and B. Tarnopol'skii, *J. Inorg. Nucl. Chem.*, 1979, **41**, 5–11.
29 K. Folting, W. E. Streib, K. G. Caulton, O. Poncelet and L. G. Hubert-Pfalzgraf, *Polyhedron*, 1991, **10**, 1639–1646.
30 R. D. Gougeon, E. B. Brouwer, P. R. Bodart, L. Delmotte, C. Marichal, J.-M. Chézeau and R. K. Harris, *J. Phys. Chem. B*, 2001, **105**, 12249–12256.
31 A. Sayari, I. Moudrakovski, J. S. Reddy, C. I. Ratcliffe, J. A. Ripmeester and K. F. Preston, *Chem. Mater.*, 1996, **8**, 2080–2088.
32 Z. Luan, D. Zhao, H. He, J. Klinowski and L. Kevan, *J. Phys. Chem. B*, 1998, **102**, 1250–1259.
33 B. Chen and Y. Huang, *Microporous Mesoporous Mater.*, 2009, **123**, 71–77.
34 C. Montes, M. E. Davis, B. Murray and M. Narayana, *J. Phys. Chem.*, 1990, **94**, 6425–6430.
35 S.-H. Chen, S.-P. Sheu and K.-J. Chao, *J. Chem. Soc., Chem. Commun.*, 1992, 1504–1505.
36 R. Szostak, in *Synthesis*, Springer, 1998, pp. 157–185.
37 W.-Y. Tsang, T. L. Amyes and J. P. Richard, *Biochemistry*, 2008, **47**, 4575–4582.
38 A. C. Reyes, X. Zhai, K. T. Morgan, C. J. Reinhardt, T. L. Amyes and J. P. Richard, *J. Am. Chem. Soc.*, 2015, **137**, 1372–1382.